Article

The influence of AlN buffer layer on the structural and chemical properties of SiC thin films produced by high-power impulse magnetron sputtering

Nierlly Galvão [1,*], Marciel Guerino [1], Tiago Campos [1], Korneli Grigorov [2], Mariana Fraga [3,*], Bruno Rodrigues [1,4], Rodrigo Pessoa [1,4], Julien Camus [5], Mohammed Djouadi [5], Homero Maciel [1,4]

[1] Centro de Ciência e Tecnologia de Plasmas e Materiais – PlasMat, Instituto Tecnológico de Aeronáutica, 12228-900, São José dos Campos, SP, Brazil.; marcielguerino@yahoo.com.br (M.G.), moreiratiago22@gmail.com (T.C.), rspessoa@ita.br (R.P.), homero@ita.br (H.M.)

[2] Space Research and Technology Institute, Acad. G. Bonchev Str. Bl.1, 1113, Sofia, Bulgaria; kgrigoro@abv.bg (K.G.)

[3] *Instituto de Ciência e Tecnologia, Universidade Federal de São Paulo (Unifesp), 12231-280, São José dos Campos, SP, Brazil*

[4] Universidade Brasil, Rua Carolina Fonseca 235, 08230-030, São Paulo, Brazil; bruno.manzolli@gmail.com (B.R.)

[5] Institut des Matériaux Jean Rouxel IMN, UMR 6502, Université de Nantes, 2 rue de La Houssinière, BP 32229, 44322 Nantes Cedex, France; jcamus@gmail.com (J.C.), abdou.djouadi@cnrs-imn.fr (M.D.)

* Correspondence: nierlly@gmail.com (N.G.), mafraga@ieee.org (M.F.)

Abstract: Many strategies have been developed for the synthesis of silicon carbide (SiC) thin films on silicon (Si) substrates by plasma-based deposition techniques, especially plasma enhanced chemical vapor deposition (PECVD) and magnetron sputtering, due to importance of these materials for microelectronics and related fields. A drawback is the large lattice mismatch between SiC and Si. The insertion of a thin aluminum nitride (AlN) buffer layer between them has been shown useful to overcome this problem. Herein, the high-power impulse magnetron sputtering (HiPIMS) technique was used to grow SiC thin films on AlN/Si substrates. Furthermore, the SiC films were also grown on Si substrates. Comparisons of the structural and chemical properties of SiC thin films grown on the two types of substrates allowed us to evaluate the influence of AlN buffer layer on such properties. The chemical composition and stoichiometry of the samples were investigated by Rutherford backscattering spectrometry (RBS) and Raman spectroscopy, while the crystallinity was characterized by grazing incidence X-ray diffraction (GIXRD). Our set of results evidenced the versatility of HiPIMS technique to produce polycrystalline SiC thin films at near room temperature only varying the discharge power. In addition, this study opens up a feasible route for the deposition of crystalline SiC films with a good structural quality using AlN buffer layer.

Keywords: HiPIMS; silicon carbide; aluminum nitride; thin film; RBS; GIXRD; Raman spectroscopy

1. Introduction

Silicon carbide (SiC) has been proved as promising material for microelectronic applications due to its excellent physical and electronic properties, such as high surface hardness, wide bandgap and high thermal conductivity at low and high temperatures [1-6]. These outstanding properties make it an attractive material for the development of harsh-environment devices such as Micro-Electro-Mechanical Systems (MEMS) and power electronics [5, 7-9].

For microelectronic device applications, it is desirable that SiC thin films to be grown on Si substrates because their manufacturing processes is based on Si microfabrication technology, which is compatible with standard industrial processes [8, 10-12]. It is difficult to grow high-quality crystalline SiC (c-SiC) films on Si substrate at low temperatures (< 300ºC) due to a large mismatch between their lattice constant (almost 20%) and thermal expansion coefficients, which usually affect

the final properties of the grown material [13]. In order to reduce these effects, a buffer layer may be added. For this purpose, aluminum nitride (AlN) thin film is frequently used since it presents a minimum mismatching in the lattice constant (less 1%) with SiC, and a similar thermal expansion coefficient [14-17].

The achievement of a good crystallinity in the SiC thin films is a desirable feature since it influences different material properties [18]. As the SiC thin films deposited at low temperature grow in amorphous or nano-crystalline structure, it is necessary a post-treatment, such as annealing, to improve the material crystallinity. Although there are several well-known techniques for synthesizing SiC thin films, their composition and final properties may vary considerably with the applied method [3, 16]. Low pressure plasma-based techniques have been extensively investigated, in special those that allow the deposition at near room temperature, such as plasma-enhanced chemical vapor deposition (PECVD) and magnetron sputtering [1, 3, 19-22]. Along with the magnetron sputtering derivations, the high-power impulse magnetron sputtering (HiPIMS) technique appears to be very attractive due to its ability of generating high density plasmas and high degree of ionization of the sputtered atoms [23-28]. These properties allow sufficient energy for the rearrangement of atoms / molecules during the growth of the film, thus facilitating the formation of crystalline phases. Some reports have demonstrated that depending on the deposition parameters and target composition, around of 50-90% of the sputtering atoms are in an ionized state [21, 25, 27]. This occurs because of the particular mechanism in which the HiPIMS power supply applies the power over the magnetron target for generating the plasma, namely high-power pulses, low frequency and low duty cycle (lower than 10%) [25, 27-29]. Interesting reviews about HiPIMS were written by Gudmundsson et al. [28] and Sarakinos et al. [27].

Despite the HiPIMS source is applied in the synthesis of various metal and semiconductor materials, there is a clear lack of studies focusing on the growing of SiC thin films using this technique. The studies related to this topic are from Ti-Si-C and SiCN films using HiPIMS [23, 30]. In the work of Alami et al. [30], the effect of process parameters such as gas pressure, substrate geometry and distance of target substrate on some properties of the as-deposited Ti-Si-C film was investigated. They observed that the Ti-Si-C film quality can be improved by HiPIMS technique [30]. Pusch et al. performed a comparison between SiCN films deposited by different target configurations and techniques, i.e. RF, DC and HiPIMS-sputtering [23]. Recently, Leal et al. deposited SiC thin film on Si by HiPIMS using SiC target [31], however, only amorphous films were obtained.

In this study, we explore the structural and chemical properties of polycrystalline SiC films grown at room temperature on Si and AlN/Si substrates by HiPIMS technique. The composition, bonding, structure and crystallinity of the samples were investigated by RBS, Raman spectroscopy and GIXRD.

2. Materials and Methods

2.1. Deposition Method

SiC thin films were grown onto polished p-type Si (100) wafers, covered or not with an AlN buffer, via HiPIMS in a high-vacuum chamber with a background pressure of 6×10^{-6} Torr. More details about the HiPIMS reactor can be found elsewhere [31, 32]. The working pressure of the argon gas (99.999%) was maintained at 3 mTorr for a corresponding flow rate of 20 sccm. The target was a commercial high-purity SiC (99.5%, Kurt J. Lesker) with diameter of 4 inches. For film growth, the power from the HiPIMS power supply (Solvix HIP^3 5kW) was 200 and 400 W. In all cases the duty cycle was fixed at 5%, freguency 500Hz and Pulse ton 100µs. In order to remove the target surface contaminants, a pre-sputtering time at 200 W, for 10 min, was performed. In addition, the substrate holder was maintained at a floating potential whereas the deposition time and the target-substrate distance were fixed at 60 min and 60 mm, respectively.

The AlN/Si substrates were provided by "Institut des Matériaux Jean Rouxel in Nantes University". In these substrates, the sputtered AlN buffer layer has a thickness around 1300 nm and main crystallographic orientation in (002). For more details, see references [33, 34].

2.2. Characterization Techniques

Rutherford backscattering spectrometry (RBS) was used to measure the elemental composition, stoichiometry and the thickness of the as-deposited SiC thin films. The measurements were carried out using a 2 MeV $4He^+$ beam from a Pelletron accelerator type with a particle detector positioned at 170° from the incident beam. The RBS spectra were analyzed using a RUMP code (RBS analysis package) developed by L. R. Doolittle from Cornell University [35].

The crystallinity of the SiC films was inferred from GIXRD with incidence angles (ω) of 1.0°, 1.5°, 2.0°, using a Philips diffractometer PW1830/1840 with CuK$_\alpha$ radiation.

For measurements of Raman spectroscopy, a model 2000 Renishaw system equipped with an Ar ion laser (514.5 nm) was used. Raman spectra were obtained at room temperature in the range of 400-1800 cm^{-1}.

3. Results and Discussion

3.1. Chemical Composition and Stoichiometry

Figure 1 shows the experimental and simulated RBS spectra of the as-deposited.

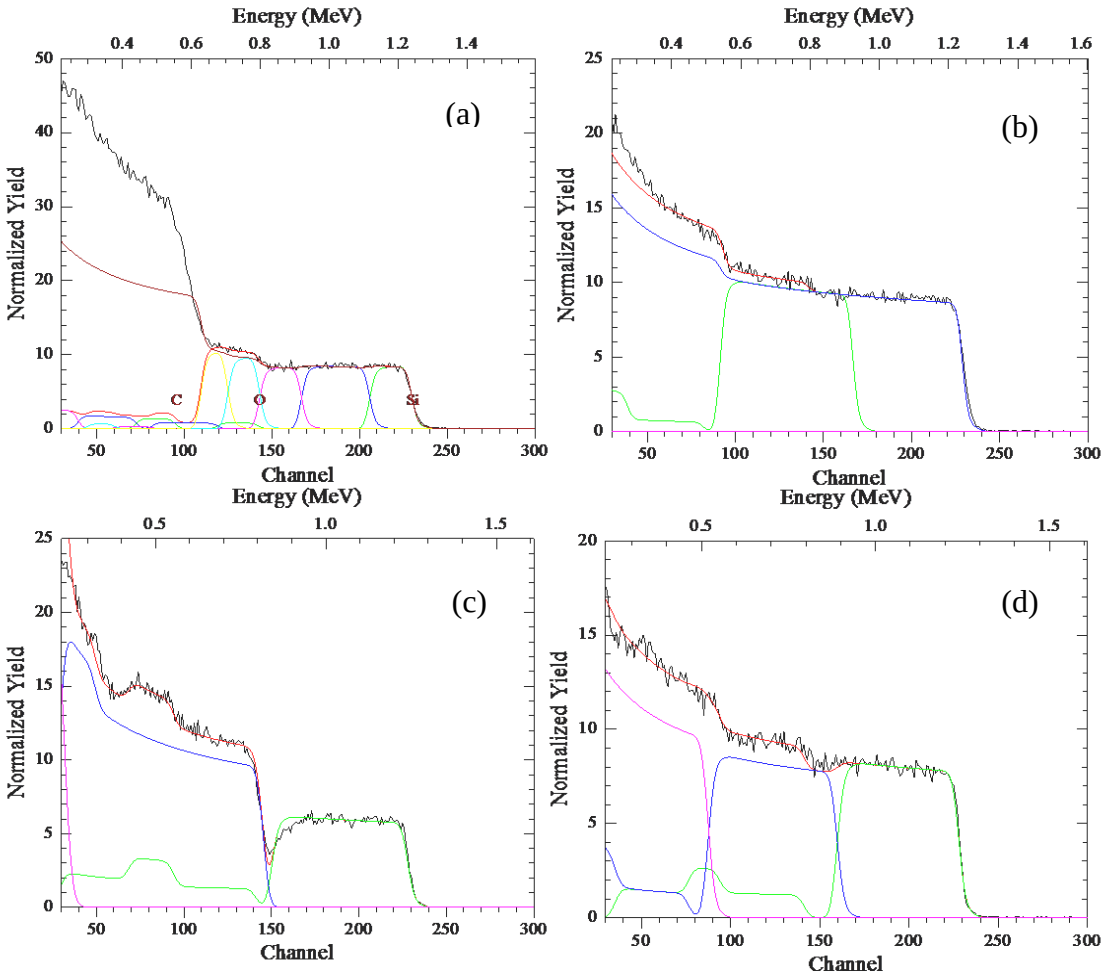

Figure 1. Experimental and simulated RBS spectra of the SiC films deposited in: (a) SiC/Si at 200 W; (b) SiC/Si at 400 W; (c) SiC/AlN/Si at 200 W and; (d) SiC/AlN/Si at 400 W. The red line represents the simulation profile and other colors represent different film layers observed by simulation.

SiC thin films on Si and AlN/Si substrates for conditions of 200 and 400 W. Table 1 summarizes the results of the RBS spectra analyzes.

Table 1. Results of the RBS analysis.

Sample	nº layers	Composition by layer[1]	Layer thickness
SiC/Si 200 W	5	1. SiC stoichiometry with less than 13% of oxygen.	1. 260 nm
		2. SiC with about 10% excess of carbon.	2. 400 nm
		3. SiC with about 50% excess of carbon.	3. 250 nm
		4. SiC stoichiometric.	4. 170 nm
		5. SiC with about 10% excess of carbon.	5. 145 nm
SiC/Si 400 W	2	1. SiC – 86%; SiO_2 phase – 4% dispersed in that volume; O – 5%; N – 5%.	1. ~ 900 nm
		2. SiC – 50%/ and SiN – 50%.	2. ~ 600 nm
SiC/AlN/Si 200 W	2	1. SiC stoichiometry– 56%; C solid state and O contamination in 44%.	1. ~ 930 nm
		2. Buffer AlN stoichiometry.	2. ~ 1300 nm
SiC/AlN/Si 400 W	2	1. SiC stoichiometry – 80% with 20 % of C solid state and O contamination in volume.	1. ~1360 nm
		2. Buffer AlN stoichiometry.	2.~ 1300 nm

[1] Layer 1 refers the layer at the top of the film.

Figure 1a depicts the spectrum of SiC deposited on Si at 200 W and the simulation reveals a film with a total thickness of approx. 1200 nm, with a highly nonhomogenous elemental distribution along the film depth. To better visualize the variation of stoichiometry along film depth the simulation was made comprising 5 sublayers, identified at Table 1. The top of the layer has a perfect stoichiometry under these deposition conditions, being 260 nm of pure SiC with less than 13% of oxygen. The middle part (approx. 400 nm) consists of SiC with 10% excess of carbon. The next 250 nm layer has about 50% carbon excess and a substantial drop of the oxygen content is observed. The next 170 nm layer is fully stoichiometric, followed by the last 145 nm layer adjacent to the Si surface, where again a 10% of carbon excess were found. Concerning the incorporated oxygen in the first analyzed layers of the SiC film, a recent work of Medeiros et al. observed an unintentional doping of SiCxNy thin films by oxygen contamination coming from the vacuum environment of a magnetron cosputtering system [32]. In this work, RBS results showed that all samples contain significant amounts of oxygen (up to 16 at. %). Further, XPS results showed that most of this oxygen is located in the film surface [32]. These results corroborate with the RBS analysis presented in Fig. 1a. In addition, Pomaska et al. presented studies on the unintentional doping by oxygen contamination. They demonstrated that the oxygen incorporation has influenced the microstructural, electronic, and optical properties of SiC films [36]. It has been shown that oxygen incorporation during the film deposition increases the crystallinity of SiC films. Fact also observed in this work.

For the SiC grown on Si at 400 W, Fig. 1b, the analysis of RBS spectra indicated that the total film thickness was around 1500 nm. The film exhibited SiC with almost pure and stoichiometric composition in depth, even so, two zones could be distinguished as presented in Table 1. Beyond SiC, SiO_2 and SiN phases, there were O and N contaminants. This sputtering condition results in heterogeneous film composition with variable elemental depth distributions. In general, the higher power deposition energy, as in this case, leads to Ar ions striking onto the film surface with high energy, which contributes for the formation of chemical phases. Of course, if different impurities act as film constituents, they are involved in the film composition forming stable bounds (SiO_2, SiN).

From the thickness results of the SiC films grown at 200 W (1200 nm) and 400 W (1500 nm), it is possible to observe that although the applied power is twice higher there was a small increase in the deposition rate for SiC films on Si substrate. In conventional sputtering processes, the deposition rate of SiC film increases linearly with sputtering power [20-21]. In general, HiPIMS has exhibited different growth mechanism and lower deposition rates than those observed for conventional

sputtering processes [27, 28, 37]. Different effects have been considered to explain the differences between DC and HiPIMS deposition rates. There are three main reasons considered [38]: (i) the less than-linear increase of the sputtering yield with increasing ion energy ion return to the target and self-sputtering, (ii) ion return to the target and self-sputtering and (iii) changes due to greater film density, limited sticking, and self-sputtering on the substrate.

For the SiC film deposited on AlN/Si at 200 W, the total film thickness was around 930 nm (Fig. 1c). The film composition is rather homogenous and consists of 56% pure SiC, the remainder 44% of the film is composed of C and O in bulk of the film. The buffer layer of AlN consists of 1300 nm thick sub-stoichiometric AlN with 5% less nitrogen, resulting in some point defects. Note in this case, that the substrate change provided the growth of a high stoichiometric SiC film. Relative to film thickness, it is evidenced from Fig. 1 and 3 that the change of Si by AlN/Si substrate promotes the decrease of SiC film thickness. Although sputtering processes have deposition rates that are independent of the substrate type, the film nucleation process and consequent crystallization and compaction is dependent. Nivedita et al. confirmed some of these observations depositing RF sputtered Fe-Ga thin films on MgO, quartz and Si substrates [39]. Indeed, in the next topic will be evidenced that the crystallization of SiC is greater for the film deposited on Si. Crystalline films tend to have greater roughness and even porosity in comparison with amorphous films, which consequently increases the final thickness [40].

Finally, the SiC thin film deposited on AlN/Si at 400 W (Fig. 1d), exhibited a high percentage of purely stoichiometric SiC film, with the presence of C and O in volume. However, for this condition the estimate of the thickness by RBS was limited due the loss of the energy via scattering, thus, upon certain limits, e.g. above channel n° 90 (Fig. 1d), the thickness could be estimated as being around 1360 nm. Ultimately, the elemental depth distribution along the film thickness was uniform, which makes the present method and process conditions very useful for the achievement of high-quality SiC thin film deposition.

3.2. Structural Analysis

Fig. 2 shows the GIXRD patterns of the as-deposited SiC thin films. By varying the GIXRD incidence angle, the film can be analyzed in depth. Fig. 2a and 2b show the patterns for grazing incidence angles of 1.0° and 1.5°, respectively. The Bragg reflections suggest the existence of α and/or β SiC nanocrystalline structures. Although the patterns exhibit the SiC phase, it is not possible to determine which of the SiC phases are present because some diffraction peaks of α and β SiC might be overlapped [41]. The carbon phase, at ~25°, is also visible and confirms the RBS results indicating an excess of C (Table 1). Lastly, two broad peaks at ~47° and 55° were assigned with as unidentified. While some studies have attributed these peaks to the SiC polymorph phase [42, 43], others often relate them as being C or Si phase [44-46]. Observing the results of GIXRD with an incidence angle of 2° (Fig. 3), and comparing with the smaller angles results, the variation of the crystalline phases with the depth of the film can be clearly noted.

In addition, Fig. 2 shows that all the patterns presented Bragg reflections, therefore suggesting the existence of SiC nanocrystalline structures achieved without substrate heating, in this case. By varying the GIXRD incidence angle, the resulting film can be analyzed in depth. A comparison between SiC/Si and SiC/AlN/Si, concerning the patterns for both angles of incidence (1 and 1.5 degree), reveals that the phase observed in approximately 36°, using 1.5° GIXRD as incidence angle, no more exists in the pattern obtained with the smallest angle (1.0°). This result points out the existence of phase and crystallinity variations with depth.

The film deposited on AlN buffer shows the dislocation of SiC peak between 35-36° in the GIXRD patterns. This dislocation can be attributed to the following reasons: (i) film stress; (ii) interference of the substrate (SiC/Si and SiC/AlN interface); or (iii) residual stress.

(a)

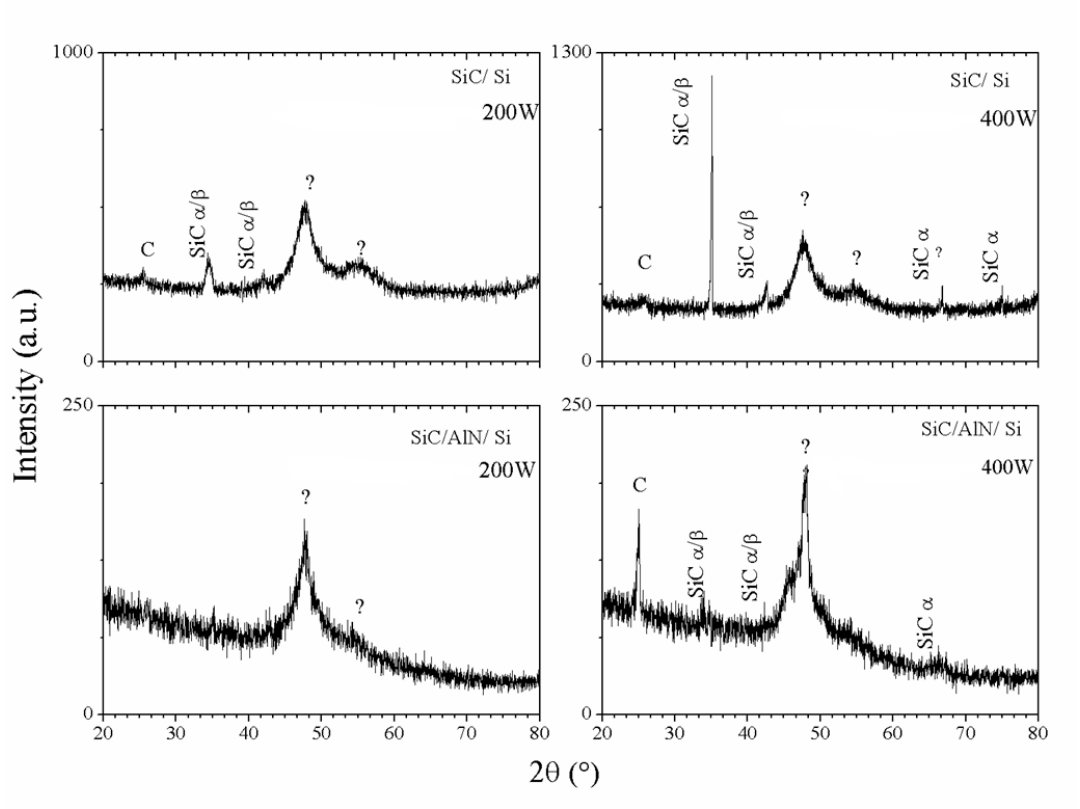

(b)

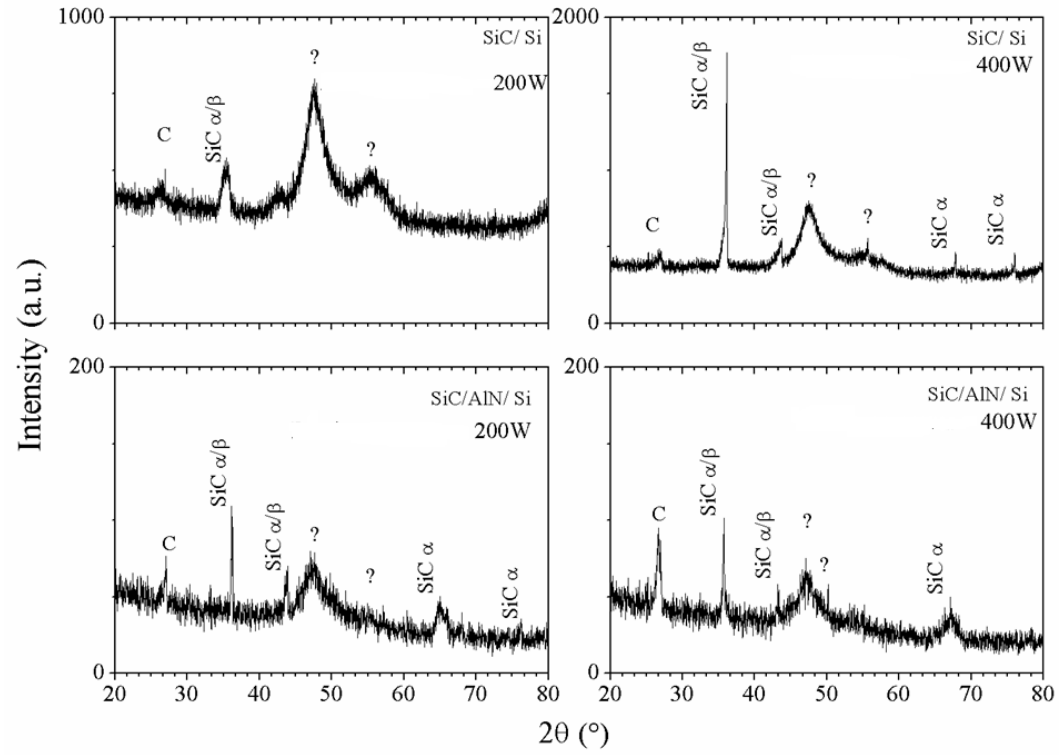

Figure 2. GIXRD patterns of the SiC thin films at grazing incidence angles: (a) ω = 1.0° and (b) ω = 1.5°.

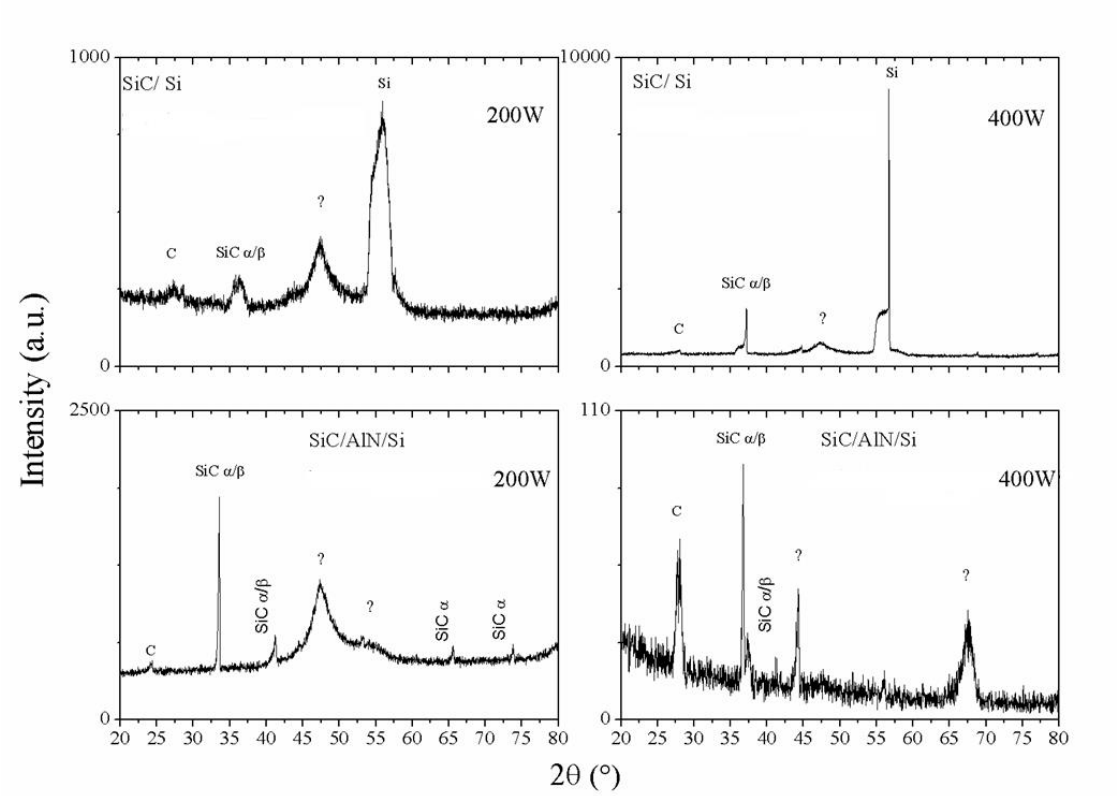

Figure 3. GIXRD patterns of the SiC thin films at grazing angle of 2°. (a) SiC film deposited by 200 W on Si substrate (b) SiC film deposited by 400 W on Si substrate, (c), SiC film deposited by 200 W on AlN buffer, and (d) SiC film deposited by 400 W on AlN buffer.

3.2. Raman Spectroscopy

Fig.4 shows the results of Raman spectroscopy used to identify the bonds present in the films. The Raman spectra for the SiC films deposited at 200 W in both substrates (with and without AlN buffer, Fig.4a) show a very visible and well-defined Si peak at 519.41 cm^{-1}. Since the thickness difference between both films is small, the substrate has an accentuated influence. In addition to Si, the SiC film deposited on AlN buffer showed i) a peak relative to AlN in ~ 652.20 cm^{-1}; ii) peaks for SiC and Si at the regions between 741-894 cm^{-1} and 906-1109 cm^{-1}, respectively; iii) and a broad carbon band at 1370-1625 cm^{-1}. Except for the AlN peak, the SiC/Si spectrum exhibited signals at the same regions of SiC/AlN/Si spectrum, however the regions relative to SiC and Si were more visible and the C bond region had a more explicit separation in two peaks (D and G band), but with low definition of the disorder band. The D band is attributed to disorder or polycrystalline carbon and the G band to the graphite like carbon [16, 46].

For 400 W (Fig. 4b), both substrates exhibited a similar behavior for the deposition of SiC films. In these spectra, the substrate signal was not detected and only peaks of C at 1457 and 1462 cm^{-1} and SiC were evident. With the exception of the spectrum of the SiC film at 200 W of SiC/Si, where the peak of the C bond was not overlapped, all spectra of the "as-deposited" SiC film showed overlapped C, D and G bands between ~1457-1462 cm^{-1}. Ferrari and Robertson [42] reported that for C–C bands, the Raman spectrum is influenced by factors such as: disorder, clustering of the sp^2 phase, presence of sp^2 C-rings or C-chains, and the ratio of sp^2 to sp^3, I(D)/I(G). Thus, with an increasing disorder of the C phase, the G peak position can be moved, and the D and G peaks will therefore overlap [16, 46, 47].

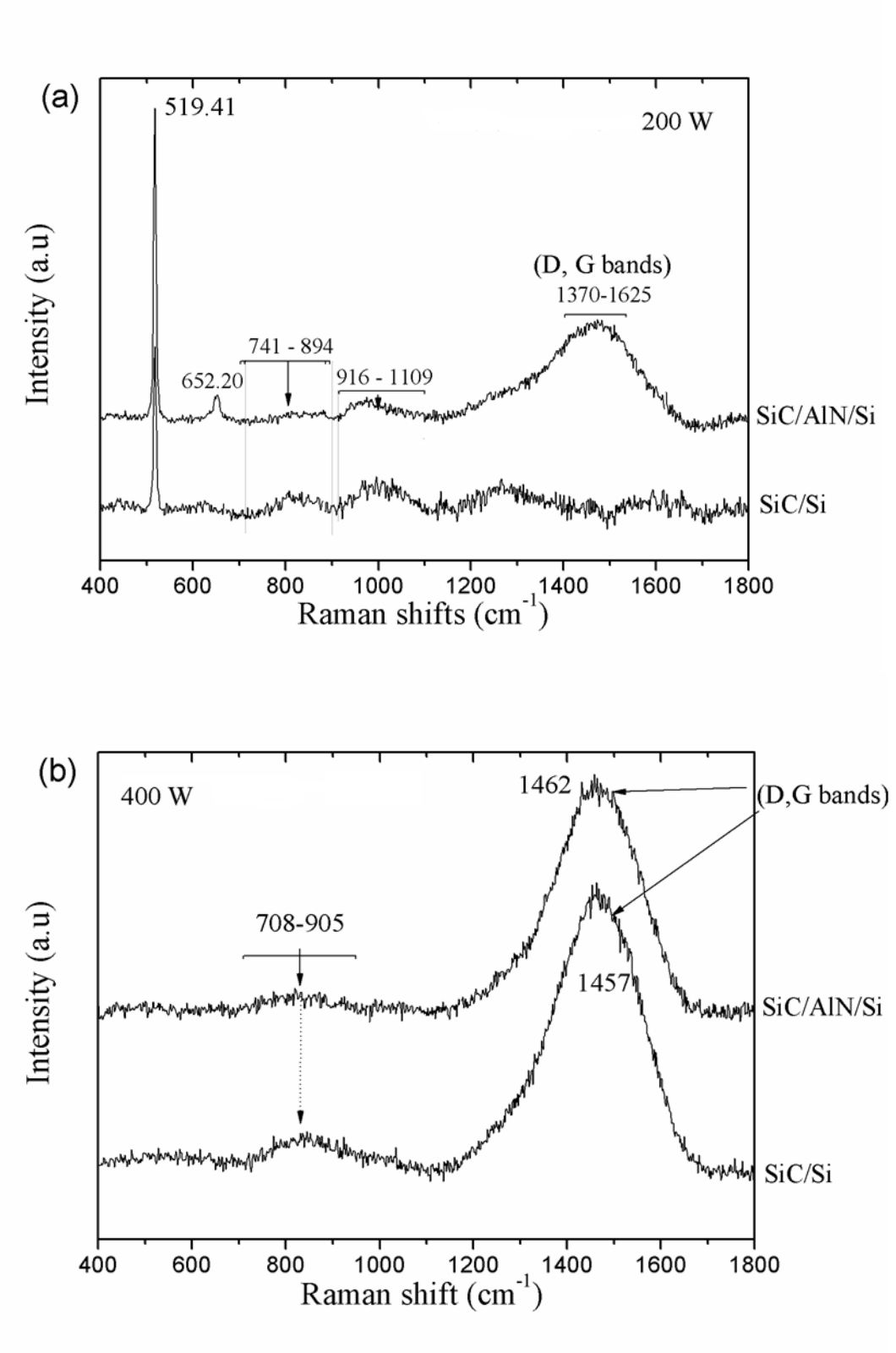

Figure 4. Raman Spectra of SiC films thin: (a) as-deposited using 200 W deposition power; (b) as-deposited using 400 W deposition power.

4. Conclusions

The influence of AlN buffer layer on the structural and chemical properties of HiPIMS SiC films grown on Si substrates were investigated using RBS, Raman spectroscopy and GIXRD. The effect of applied power (200W and 400W) was also considered. It has been observed that the HiPIMS SiC films

can exhibited a complex growth mechanism, depending on the process parameter, which led to the formation of films with inhomogeneous composition along the depth for Si and a homogeneous composition for AlN/Si substrate. This can be verified by GIXRD using three different incidence angles (1°,1.5° and 2°) which besides confirming the RBS results also evidenced the variation of crystallinity with the depth of the film. Raman spectroscopy analysis indicated the presence of Si–C bonds and that the C-C bond region was more separated in two peaks (D and G band), but with a low definition of the disorder band. In summary, the results demonstrated that the HiPIMS technique and the use of AlN buffer layer allowed for the deposition of crystalline SiC films of good quality, without need of substrate heating, with approx. 1.5 μm (at 400 W) in only 60 min, i.e., at a deposition rate of 25 nm min-1. Due to good chemical and physical properties the HiPIMS SiC films deposited on AlN/Si substrate can be used in nanotechnological applications, for example, recently we proposed the thermal decomposition of SiC thin films using CO_2 laser beam without vacuum chamber for graphene synthesis. The use of AlN buffer layer showed to be important because reduces the thermal stress between SiC and Si materials [48]. Other applications will be subject of further works.

Author Contributions: N.G., M.G., T.C., K.G., R.P. and J.C. provide the investigation and methodology, N.G., K.G., M.F., B.R., R.P., M.D. and H.M. write the original draft.

Funding: The financial support of Brazilian agency program FAPESP/MCT/CNPq-PRONEX (grant nº 11/50773-0), MCTI/CNPq/Universal (grants nº 459688/2014-6, 437921/2018-2 and 421317/2018-3), FAPESP (grant nº 18/01265-1 and 14/18139-8), CAPES/ITA (process No. 23038.005802/2014-98), CAPES/PVE (process N° No. 88881.064970/2014-01 and BEX9796/12-6), PNPD-CAPES and CNPq (grants nº 305496/2012-3 and 446545/2014-7) are also strongly acknowledged.

Acknowledgments: We would like to thank LAS-INPE for the Raman spectroscopy and GIXRD measurements, and LAMFI-USP for the RBS measurements. The authors also thank Dr. Julio César Sagas from UDESC-Santa Catarina/Brazil for discussions and operation of the HiPIMS reactor.

Conflicts of Interest: The authors declare no conflict of interest.

References

1. Rajab, S.M.; Oliveira, I. C.; Massi, M.; Maciel, H. S.; Santos Filhos, S. G.; Mansano, R. D. Effect of the thermal annealing on the electrical and physical properties of SiC thin films produced by RF magnetron sputtering. Thin Solid Films **2006,** 515, 170-175.
2. Fraga, M.A.; Furlan, H.; Pessoa, R.S.; Massi, M. Wide bandgap semiconductor thin films for piezoelectric and piezoresistive MEMS sensors applied at high temperatures: an overview. Microsystem Technologies **2014**, 20(1), 9-21.
3. Pessoa, R.S.; Fraga, M.A.; Santos, L.V.; Massi, M.; Maciel, H.S. Nanostructured thin films based on TiO_2 and/or SiC for use in photoelectrochemical cells: A review of the material characteristics, synthesis and recent applications. Materials Science in Semiconductor Processing **2015**, 29, 56-68.
4. Maboudian, R.; Carraro, C.; Senesky, D.G.; Roper, C.S. Advances in silicon carbide science and technology at the micro- and nanoscales. J. Vac. Sci. Technol. A **2013**, 31, 050805.
5. Müller, G.; Krötz, G.; Niemann, E. SiC for sensors and high-temperature electronics. Sensors and Actuators A: Physical **1994**, 43(1-3), 259-268.
6. Huang, J.; Wang, L.; Wen, J.; Wang, Y.; Lin, C.; Ostling, M. Effect of annealing on SiC thin films prepared by pulsed laser deposition. Diamond and Related Materials **1999**, 8, 2099-2102.
7. Ledermann, N.; Baborowski, J.; Muralt, P.; Xantopoulos, N.; Tellenbach, J. Sputtered silicon carbide thin films as protective coating for MEMS applications. Surface and Coatings Technology **2000**, 125, 246-250.
8. Sarro, P.M. Silicon carbide as a new MEMS technology. Sensors and Actuators A: Physical **2000**, 82(1-3), 210-218.
9. Fraga, M.A.; Pessoa, R.S.; Massi, M.; Maciel, H.S. Applications of SiC-Based Thin Films in Electronic and MEMS Devices. In Physics and Technology of Silicon Carbide Devices, 1 ed.; Yasuto Hijikata, InTech, Rijeka, Croatia, 2012, pp. 313-336.

10. Roumié, M.;Tabbal, M.; Nsouli, B.; Said, A. Determination of stoichiometry in silicon carbide materials using elastic backscattering spectrometry. Nuclear Instruments and Methods in Physics Research B **2007**, 260, 637–641.
11. Tabbal, M.; Said, A.; Hannoun, E.; Christidis, T. Amorphous to crystalline phase transition in pulsed laser deposited silicon carbide. Applied Surface Science **2007,** 253, 7050–7059.
12. Zhao, Y.M.; Sun, G.S.; Liu, X.S.; Li, J.Y.; Zhao, W.S.; Wang, L.; Li, J. M.; Zeng, Y.P. Heteroepitaxial Growth of 3C-SiC on Si (111) Substrate Using AlN as a Buffer Layer. Materials Science Forum **2009**, 600-603, 251-254.
13. Severino, A. 3C-SiC epitaxial growth on large area silicon: thin films. In: Silicon Carbide Epitaxy, 1ed, Francesco La Via, Research Singpost, Kerala, India,2012, pp. 145-191.
14. Chung, G.S.; Chung, J.M.; Lee, T.W. Deposition of AlN thin films on Si substrates using 3C-SiC as buffer layer by reactive magnetron sputtering. Electronics Letters **2008,** 44(17), 1034-1035.
15. Nakazawa, H.; Suemitsu, M. Low-temperature formation of an interfacial buffer layer using monomethylsilane for 3C–SiC/Si (100) heteroepitaxy Applied Physics Letters **2001**, 79, 755.
16. Huang, S.Y.; Xu, S.; Long, J.D.; Sun, Z.; Chen, T. Plasma-reactive SiC quantum dots on polycrystalline AlN films. Physics of Plasmas **2006,** 13(2), 023506.
17. Jeong, J.; Jang, K.; Lee, H.S.; Chung, G.; Kim, G. Raman scattering studies of polycrystalline 3C-SiC deposited on SiO_2 and AlN thin films. Physica B: Condensed Matter **2009**, 404(1), 7-10.
18. Fraga, M.A.; Pessoa, R.S.; Maciel, H.S.; Massi, M. Recent Developments on Silicon Carbide Thin Films for Piezoresistive Sensors Applications. In Silicon Carbide - Materials, Processing and Applications in Electronic Devices, Moumita Mukherjee, InTech, Rijeka, Croatia, 2011, pp. 369-388.
19. Tang, H.; Tan, S.; Huang, Z.; Dong, S.; Jiang, D. Surface morphology of α-SIC coatings deposited by RF magnetron sputtering. Surface and Coatings Technology **2005**, 197, 161-167.
20. Gou, L.; Qi, C.; Ran, J.; Zheng, C. SiC film deposition by DC magnetron sputtering. Thin Solid Films **1999**, 345, 42-44.
21. Medeiros, H.S.; Pessoa, R.S.; Maciel, H.S.; Massi, M.; Tezani, L.L.; Leal, G.; Galvão, N. K. A. M.; da Silva Sobrinho, A.S. Amorphous Silicon Carbide Thin Films Deposited by Magnetron Co-Sputtering: Effect of Applied Power and Deposition Pressure on Film Characteristics. ECS Transactions **2012**, 49, 375-382.
22. Lei, Y. M.; Yu, L.H.; Cheng, L. L.; Ren, C. X.; Zou, S. C.; Wong, S. P.; Chen, D. H.; Wilson, I. H. IR studies of reactive DC magnetron sputtered SiC films on silicon using effective medium theory Materials Letters **2000**, 43, 215-219.
23. Pusch, C.; Hoche, H.; Berger, C.; Riedel, R.; Ionescu, E.; Klein, A. Influence of the PVD sputtering method on structural characteristics of SiCN-coatings — Comparison of RF, DC and HiPIMS sputtering and target configurations. Surface and Coatings Technology **2011**, 205, s119-s123.
24. Bräuer, G.; Szyszka, B.; Vergo, M.; Bandorf, R. Magnetron sputtering – Milestones of 30 years. Vacuum **2010**, 84, 1354-1359.
25. Anders, A. Influence of the PVD sputtering method on structural characteristics of SiCN-coatings — Comparison of RF, DC and HiPIMS sputtering and target configurations. Surface and Coatings Technology **2010,** 204, 2864-2868.
26. Aijaz, A.; Lundin, D.; Larsson, P.; Helmersson, U. Dual-magnetron open field sputtering system for sideways deposition of thin films. Surface and Coatings Technology **2010,** 204, 2165-2169.
27. Sarakinos, K.; Alami, J.; Konstantinidis, S. High power pulsed magnetron sputtering: A review on scientific and engineering state of the art. Surface and Coatings Technology **2010,** 204, 1661-1684.
28. Gudmundsson, J.T. The high power impulse magnetron sputtering discharge as an ionized physical vapor deposition tool. Vacuum **2010**, 84, 1360-1364.
29. Alami, J.; Bolz, S.; Sarakinos, K. High power pulsed magnetron sputtering: Fundamentals and applications. Journal of Alloys and Compounds **2009,** 483, 530-534.
30. Alami, J.; Eklund, P.; Emmerlich, J.; Wilhelmsson, O.; Jansson, U.; Högberg, H.; Hultman, L.; Helmersson, U. High-power impulse magnetron sputtering of Ti–Si–C thin films from a Ti3SiC2 compound target. Thin Solid Films **2006**, 515(4), 1731-1736.
31. Leal, G.; Campos, T. M. B.; da Silva Sobrinho, A.S.; Pessoa, R. S.; Maciel, H.S.; Massi, M. Characterization of SiC thin films deposited by HiPIMS. Materials Research **2014**, 17(2), 472-476.
32. Medeiros, H. S.; Pessoa, R. S.; Sagas, J.C.; Fraga, M.A.; Santos, L.V.; Maciel, H.S.; Massi, M.; da Silva Sobrinho, A.S.; Costa, M. E. H. M. Effect of nitrogen content in amorphous SiCxNyOz thin films deposited

by low temperature reactive magnetron co-sputtering technique. Surface and Coatings Technology **2011,** 206 ,1787-1795.

33. Belkerk, B.E.; Soussou, A.; Carette, M.; Djouadi, M.A.; Scudeller, Y. Structural-dependent thermal conductivity of aluminium nitride produced by reactive direct current magnetron sputtering. Applied Physics Letters **2012,** 101, 151908.
34. Aissa, K. A.; Achour, A.; Camus, J.; Brizoual, L.L.; Jouan, P.; Djouadi, A. Comparison of the structural properties and residual stress of AlN films deposited by dc magnetron sputtering and high power impulse magnetron sputtering at different working pressures. Thin Solid Films **2014**, 550 264-267.
35. Doolittle, L.R. Algorithms for the rapid simulation of Rutherford backscattering spectra. Nuclear Instruments and Methods in Physics Research Section B: Beam Interactions with Materials and Atoms **1985**, 9(3), 344-351.
36. Pomaska, M.; Mock, J.; Köhler, F.; Zastrow, U.; Perani, M.; Astakhov, O.; Cavalcoli, D.; Carius, R.; Finger, F.; Ding, K. Role of oxygen and nitrogen in n-type microcrystalline silicon carbide grown by hot wire chemical vapor deposition. Journal of Applied Physics **2016** 120, 225105.
37. Diyatmika, W.; Liang, F.; Lou, B.; Lu, J.; Sun, D.; Lee, J. Superimposed high power impulse and middle frequency magnetron sputtering: Role of pulse duration and average power of middle frequency. Surface and Coatings Technology **2018**, 352, 680-689.
38. Anders, A. Deposition Rates of High Power Impulse Magnetron Sputtering: Physics and Economics Journal of Vacuum Science & Technology A **2010**, 28(4), 783.
39. Nivedita, L.R.; Kumar, V. V. S.; Asokan, K.; Rajendrakumar, R.T. Growth and Magnetic Properties of RF Sputtered Fe-Ga Thin Films. Materials Research **2015**, 18(5), 946-952.
40. Puurunen,R.L.; Sajavaara, T., Santala,, E.; Miikkulainen, V.; Saukkonen, T.; Laitinen, M.; Leskela,M. J. Nanosci. Nanotechnol. **2011**, 11, 8101-8107.
41. Li, W.; Yuan, J.; Lin, Y.; Yao, S.; Ren, Z.; Wang, H.; Wang, M.; Bai J. The controlled formation of hybrid structures of multi-walled carbon nanotubes on SiC plate-like particles and their synergetic effect as a filler in poly(vinylidene fluoride) based composites. Carbon **2013**, 51, 355-364.
42. Badini, C,; Fino, P.; Ortona, A.; Amelio, C. High temperature oxidation of multilayered SiC processed by tape casting and sintering. Journal of the European Ceramic Society **2002**, 22(12), 2071-2079.
43. Wilhelm, M.; Wruss, W. Influence of annealing on the mechanical properties of SiC–Si composites with sub-micron SiC microstructures. Journal of the European Ceramic Society **2000**, 20 (8), 1205-1213.
44. Xia, A.; Huizhao, Z.; Li, Y.; Chengshan, X. Formation of carbon nanowires by annealing silicon carbide films deposited by magnetron sputtering. Applied Surface Science **2002**, 193, 87-91.
45. Yang, W. S.; Biamino, S.; Padovano, E.; Pavese, M.; Marchisio, S.; D'Amico, G.; Mio, S.C.; Chen, X.; Fino, P.; Badini, C. Thermophysical properties of SiC multilayer prepared by tape casting and pressureless sintering. Composite Structures **2013**, 96, 469-475.
46. Kuenle, M.; Janza, S.; Eibl, O.; Berthold, C.; Presser, V.; Nickel, K.-G. Thermal annealing of SiC thin films with varying stoichiometry. Materials Science and Engineering B **2009**, 159-160, 355-360.
47. Ferrari, A.C.; Robertson, J. Interpretation of Raman spectra of disordered and amorphous carbon. Physical Phys. Rev. B **2000**, 61, 14095-14107.
48. Galvão, N.; Vasconcelos, G.; Pessoa, R.; Machado, J.; Guerino, M.; Fraga, M.; Rodrigues, B.; Camus, J.; Djouadi, A.; Maciel, H. A Novel Method of Synthesizing Graphene for Electronic Device Applications Materials **2018** 11(7), 1120.